Identification of an Optimized Heating and Fast Ion Generation Scheme for the Wendelstein 7-X Stellarator

H. W. Patten[1,†] J. P. Graves[1] W. A. Cooper[1] J. Eriksson[2] D. Pfefferlé[3] W7-X team[4] and JET contributors[5,*]
[1]Ecole Polytechnique Fédérale de Lausanne (EPFL), Swiss Plasma Center (SPC), CH-1015 Lausanne, Switzerland
[2]Department of Physics and Astronomy, Uppsala University, SE-75120 Uppsala, Sweden
[3]University of Western Australia, 6009 Crawley, Australia
[4]Max-Planck-Institut für Plasmaphysik, EURATOM Association, Wendelsteinstrasse 1, 17491 Greifswald, Germany
[5]EUROfusion Consortium, JET, Culham Science Centre, Abingdon OX14 3DB, United Kingdom

(Received 4 July 2019; revised manuscript received 24 December 2019; accepted 3 March 2020; published 15 April 2020)

A Doppler shifted resonance minority species ion cyclotron range of frequency (ICRF) scheme for heating neutral beam ions has been identified and optimized for the Wendelstein 7-X stellarator. Compared with more conventional methods, the synergetic scheme increases the normalized core collisional power transfer to the background plasma, and induces larger concentrations of energetic ions. Simulations in the intricate 3D magnetic stellarator geometry reveal an energetic distribution function that is only weakly anisotropic, and is thus relevant to fast ion and alpha particle driven Alfvén eigenmode experimental preparation. Quasilinear theory and simulations of the Joint European Torus indicate that the excellent confinement properties are due to increased velocity diffusion from ICRF interaction along the magnetic field lines. Agreement is found between SCENIC simulations and Joint European Torus experimental measurements for the total neutron rate and the energy distribution of the fast ions.

DOI: 10.1103/PhysRevLett.124.155001

The advanced stellarator Wendelstein 7-X (W7-X) has recently performed beyond expectations in its initial plasma operations [1,2]. The development of the stellarator towards a commercial fusion reactor must demonstrate efficient core-localized plasma heating schemes and energetic ion confinement, despite the 3D structure of the stellarator magnetic fields. Improving the performance and efficiency of auxiliary heating schemes leads directly to improved commercial reactor designs, a key focus of ongoing research. A crucial final challenge for advanced stellarators is to demonstrate that fusion born alpha particles could remain confined in the plasma for long enough to achieve sustained thermonuclear burn. It is noted that such ions carry the potential hazard of driving instabilities such as toroidal Alvén eigenmodes (TAEs) [3], and these modes in turn can cause the ejection of the resonant alpha particles, thus compromising fusion power. It is therefore a high priority that current devices discover a means of generating large numbers of superthermal ions, so that confinement and stability studies can be made empirically. In current tokamak and stellarator plasmas, ion cyclotron range of frequency (ICRF) heating is used to heat the plasma core and generate superthermal ions. Certain new ICRF schemes, known generally as three-ion species heating schemes, have been proposed [4] for this purpose. Nevertheless, it has been recently shown [5,6] that superthermal ions with $E >$ 60 keV produced by such schemes have very low concentrations in W7-X due to its intrinsically high collisionality (highly dense plasma), and the fact that such schemes generate preferentially deeply trapped particles, which have the worst confinement properties in strongly 3D magnetic fields [7]. Neutral beam injection (NBI) in W7-X [8] does not generate ions with sufficient energy to verify magnetic confinement of superthermal trapped ions [9,10].

In this Letter, a synergetic ICRF-NBI heating method is applied to the Joint European Torus (JET) tokamak and to W7-X. We show that this Doppler-shifted resonance minority species ^{4}He(H) synergetic ICRF heating of hydrogen NBI ions in the optimized high mirror W7-X plasma equilibrium helps to improve energetic NBI ion confinement and further accelerate the injected beam ions. ICRF theory and simulations of JET experiments [11] using the SCENIC code [12] illustrate why the application of the Doppler-shifted resonance minority species ICRF-NBI heating scenario can be expected to be beneficial for the W7-X device. Validation of the SCENIC code against JET experimental data establishes important parametrization of the code, and establishes confidence in the promising predictions for W7-X.

The resonance condition for ICRF is defined as

$$\omega_a = n\Omega_{c,\alpha} + k_\parallel v_{\parallel,\alpha}, \quad (1)$$

with ω_a the antenna frequency, n the harmonic number, the cyclotron frequency $\Omega_{c,\alpha} = Z_\alpha B/m_\alpha$ of the species α, Z_α is the effective charge, m_α the particle mass, and B the magnetic field strength. Standard on-axis ($\omega_a = \Omega_c$) ICRF scenarios apply fundamental $n = 1$ heating of thermal particles and second harmonic schemes apply $n = 2$. More efficient ICRF heating maximizes the rf-wave polarization, where the polarization is defined as E^+/E^-, referring to the components of the ICRF wave rotating in the direction of the ions and electrons, respectively. Experimental and modeling efforts into synergetic ICRF-NBI heating in tokamaks, similar to the schemes developed in this Letter for the W7-X stellarator, can be found in Refs. [11,13–17]. In particular, JET experiments in Ref. [13] applied the on-axis fundamental ICRF to majority deuterium NBI. Fundamental heating of a majority species results in low polarization at the thermal resonance $\omega_a \sim \Omega_{c,\alpha}$. The large Doppler shift of the NBI ions permits efficient polarization and thus improved rf-power transfer, but away from the core (due to the on-axis rf frequency), resulting in poor overall rf heating and fast ion generation. An alternative approach using on-axis second harmonic $n = 2$ heating in JET and ASDEX of majority deuterium NBI species was reported in Refs. [14–17]. rf-heating efficiency for $n > 1$ minority species heating depends on finite Larmor radius (FLR) effects for rf-power absorption and thus performance decreases for increasing n, and rf interaction occurs with fewer particles than fundamental heating.

Building on this previous experimental knowledge, a synergetic ICRF-NBI scheme is developed in this Letter to improve the core rf heating over the on-axis scenarios previously mentioned. In this fundamental heating scenario, the antenna frequency is modified such that only NBI ions with large $v_\parallel$ resonate on axis in front of the antenna through the Doppler-shift effect, limiting thermalized NBI ion resonance to off axis. For this scheme, the NBI beam species is ensured to remain a minority plasma species, and the majority background ion species must have a different charge-to-mass ratio to that of the NBI ions for enhanced rf polarization. The inverted Doppler-shifted minority species synergetic ICRF-NBI scenario experiments reported in Ref. [11] are a particular case of the scheme proposed in this Letter. In contrast to Ref. [11], the synergetic ICRF-NBI heating scheme proposed here does not limit the heating scheme to an inverted scenario, which refers to when the charge-to-mass ratio of the majority species is larger than the minority species. For large minority ion concentrations in inverted scenarios, parasitic electron rf-power absorption tends to dominate [18]. The inverted scenario described in Ref. [11] avoids this problem by adjusting the rf-antenna frequency so that the energetic NBI ions absorb the rf power instead of the electrons, making it more sensitive to variations in ω_a and the concentration of thermalized NBI ions. The scheme is referred to as a three-ion species scheme in Ref. [11]. A more precise description is used in this Letter to account for the NBI beam distribution as a slowing down distribution and not a delta function in velocity space, the former resulting in one broad and not two distinct resonant regions between the thermal and NBI ions. As a final point on the historical review on ICRF heating of NBI ions, Kolesnichenko *et al.* [19] investigated a form of synergetic RF-NBI for improved NBI confinement. Synergetic ICRF-NBI scenarios in W7-X were predicted to be unable to improve NBI confinement at high magnetic field ($B_0 = 2.5T$) in Ref. [19] due to rf antenna design limitations. The opposite conclusion is found in this Letter, by including more realistic physics in the calculation via use of the SCENIC [12] numerical code package. Our approach avoids many of the approximations made in Ref. [19], such as no 3D dependence in $k_\parallel$, simplified magnetic geometry, no Coulomb collisions, cold plasma approximation, ideal MHD waves, simplified rf antenna and NBI geometries, and no finite orbit width (FOW) effects. A description of the methodology for synergetic ICRF-NBI heating with the SCENIC package is given in Ref. [20], Sec. 5.2, under "fast-splitting method."

Modeling of wave-particle interactions with a quasilinear operator (QLO) and the corresponding velocity space diffusion in magnetized plasmas was originally presented in Ref. [21]. The QLO can be used to relate a change in the resonant species distribution function in time to that of the diffusion of particles in velocity space:

$$\frac{df_\alpha}{dt} = \frac{\partial}{\partial \mathbf{v}} \cdot \left(\mathcal{Q} \cdot \frac{\partial f_\alpha}{\partial \mathbf{v}} \right) + \sum_\beta \mathcal{C}[f_\alpha, f_\beta] + \mathcal{S} - \mathcal{L}, \quad (2)$$

where $f_\alpha(\vec{x}, \vec{v}, t)$ is the distribution function of the resonant particle population, $\mathcal{Q}$ the quasilinear diffusion operator, $\mathcal{C}$ the collisionality with the background, and particle source and losses are $\mathcal{S}$ and $\mathcal{L}$, respectively. Upon interaction with the ICRF wave through $\mathcal{Q}$, the change in parallel velocity of the particle is related to the change in the perpendicular velocity by [22]

$$\frac{dv_\parallel}{dv_\perp} = \frac{v_\perp}{v_\parallel} \left(\frac{\omega_a}{n\Omega_c} - 1 \right). \quad (3)$$

Equation (3) goes to zero for on-axis ICRF heating of isotropically distributed thermal ions ($v_\parallel \sim v_\perp$, $\omega_a = \Omega_c$), producing trapped particle populations. In contrast, the shifted antenna frequency $\omega_a = \Omega_c + k_\parallel v_\parallel$ implemented for this synergetic heating scheme increases $v_\parallel$ diffusion and generates more isotropic resonant ion populations [19,22]. For a given ω_a and over a localized region in

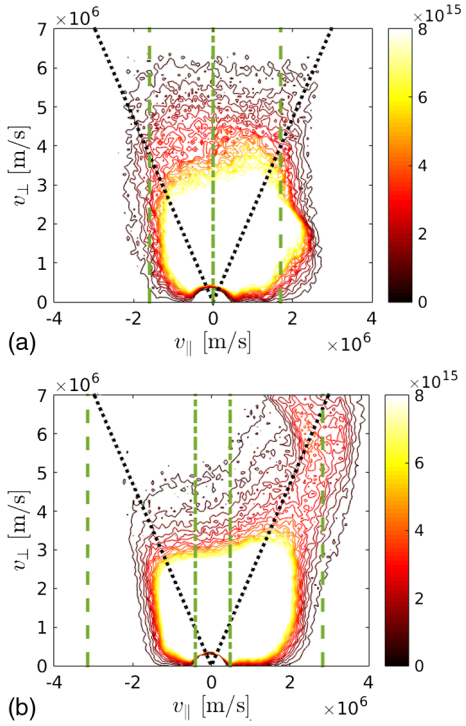

FIG. 1. 2D contour plots illustrating the resulting velocity space distribution for core localized particles with $s < 0.15$ of (a) on-axis $\omega_a = 21$ MHz and (b) off-axis Doppler-shifted $\omega_a = 25$ MHz minority species ICRF-NBI heating scenarios in JET. The dashed black line represents the trapped-passing boundary, and the vertical green lines represent the upper (dashed) and lower (dot-dashed) $v_\parallel$ limits of particle resonance according to Eq. (4).

space, wave-particle resonance occurs over a finite range of $v_\parallel$:

$$v_{\parallel,\mathrm{res}} \in \left[\min_{\{k_\parallel^+,\Omega\}}\left(\left|\frac{\omega_a-\Omega}{k_\parallel^+}\right|\right), \max_{\{k_\parallel^+,\Omega\}}\left(\left|\frac{\omega_a-\Omega}{k_\parallel^+}\right|\right)\right] \cup \left[-\max_{\{k_\parallel^-,\Omega\}}\left(\left|\frac{\omega_a-\Omega}{k_\parallel^-}\right|\right), -\min_{\{k_\parallel^-,\Omega\}}\left(\left|\frac{\omega_a-\Omega}{k_\parallel^-}\right|\right)\right]. \quad (4)$$

The upper limit in $|v_{\parallel,\mathrm{res}}|$ is larger for ICRF-NBI than standard minority species heating.

To illustrate the distinctive mechanism of increased $v_\parallel$ diffusion, simulations are made for the JET tokamak experiment pulse 91 256, described in Ref. [11]. The plasma profiles were averaged over 10.5 ± 0.15 s. The on-axis plasma parameters simulated are $n_e = 4.1 \times 10^{19}$ and $T_e = 4.1$ keV, with the assumption $T_i \sim T_e$. The total deuterium content $X[D_{\mathrm{th}}]$ of the JET $(D)H$ experiment is predicted to be ~10%–20%. The NBI power was 3.5 MW and ICRF power was 1.3 MW at this time. In addition to the JET relevant Doppler-shifted (off axis) ICRF-NBI heating with $\omega_a(\text{off axis}) = 25$ MHz, simulations with standard on-axis minority species ICRF-NBI heating $\omega_a(\text{on axis}) = 21$ MHz are made. While mode conversion effects [18] are

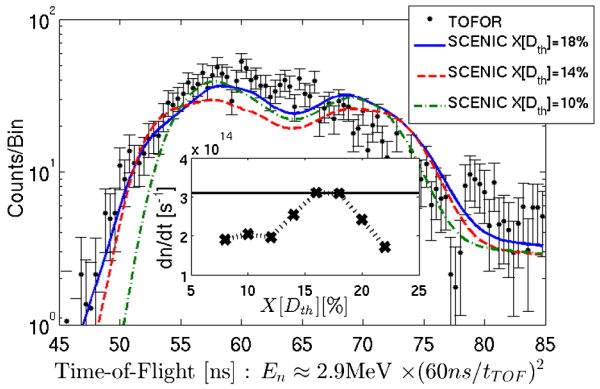

FIG. 2. Counts per bin [a.u.] of the time of flight, comparing TOFOR (taken over $t = 9$–11.5 s) plotted as points with error bars with the normalized SCENIC results, where the simulations $X[D_{\mathrm{th}}] = 10\%$, 14%, and 18% are plotted as green dot-dashed, red dashed, and solid blue lines, respectively. The inset plot indicates the total neutron rate as a function of $X[D_{\mathrm{th}}]$ (dashed line) and the experimental total neutron count $\sim 3.1 \times 10^{14}$ (solid line).

not fully resolved in these simulations, Fig. 1 provides an illustrative comparison of the velocity space distribution of the on-axis and off-axis simulations. The vast majority of the highly energetic particles generated by the JET Doppler-shifted $\omega_a(\text{off axis}) = 25$ MHz synergetic minority species ICRF-NBI scheme are passing. This is also reflected by the anisotropy in $v_\parallel$. In contrast, energetic particles produced by the on-axis $\omega_a(\text{on axis}) = 21$ MHz scheme have significantly lower $v_\parallel$ and are approximately symmetric. The vertical green lines, calculated using Eq. (4), illustrate the possible regions of ICRF resonance for a given range of values of $k_\parallel^{+/-}$ and Ω. Trapped thermal particles are prevented from resonating on axis for the Doppler-shifted scheme, contrary to on-axis heating.

The fast ion distribution function obtained from the SCENIC JET simulations is validated against neutron diagnostic measurements of pulse 91 256. The simulations are sensitive to the core deuterium concentration $X[D]$, which is not directly known empirically. The edge concentration is measured to be 8%–9% at the time of interest, while the total concentration, estimated to be 10%–20%, can be more accurately identified via sequences of SCENIC simulations and the neutron diagnostics as explained now. The JET time-of-flight neutron spectrometer TOFOR diagnostic [23] measures the time delay for a neutron to pass between two detectors, inferring neutron energy. Figure 2 plots the normalized neutron count distribution of SCENIC simulations against the TOFOR measurements, illustrating that the results are in agreement with the measurements made by the TOFOR diagnostic for $14 < X[D] < 20\%$. Within this range, the energetic NBI ion concentration was self-consistently calculated to be $X[D_{\mathrm{NBI}}] \sim 1\%$. The inset figure shows the total neutron

rate, calculated using D-D beam-thermal interactions [24] and beam-beam interactions [25], noting that the experimental total neutron rate averaged over $t = 10.5 \pm 0.15$ s is 3.1×10^{14} neutrons per second [see Fig. 3(d) of Ref. [11]], shown as the solid black line in the inset plot. The total neutron count shown in the inset plot provides additional evidence, alongside the neutron time-of-flight distribution comparison with TOFOR, that best agreement is for total deuterium concentration $14 < X[D] < 20\%$. Having verified SCENIC simulations of the inverted $(D)H$ Doppler-shifted resonance minority species ICRF-NBI heating scheme against JET experimental data, we now simulate the noninverted ^{4}He(H) scheme in W7-X.

ICRF intuition in the scientific community has largely been developed from tokamak experiments and modeling. In a tokamak, the ICRF resonant surface is approximately defined by a particular major radius R. In stellarators, however, the magnetic field strength varies as a function of the toroidal angle along the magnetic axis. The resonant surface becomes highly 3D, and on-axis resonance is only achieved for a limited range of toroidal angles for the high mirror equilibrium. Particle trapping in magnetic loss wells found in W7-X is not present in toroidally axisymmetric geometries. The 3D waves, particle orbits, and resonant interactions inherent in the SCENIC code take such complexities into account. For the W7-X simulations, the on-axis electron density and temperature is 1.5×10^{20} m^{-3} and 4 keV, respectively, and the total plasma energy content is 1.9 MJ. Plasma profiles and the magnetic equilibrium are given in Ref. [6]. The high mirror W7-X geometry has been optimized at high plasma β for a variety of different properties, i.e., to reduce the induced bootstrap current, divertor heating, turbulent transport, and for confinement of fast trapped particles [26]. The NBI power is 6.84 MW and ICRF power is 1.5 MW, with $\omega_a = 38$ MHz. For consistency with the JET experiments, the thermal hydrogen concentration in the W7-X simulations is taken to be ~18%. It is found that $X[H_{\rm th}]$ does not strongly influence the collisional power transfer, nor the number of energetic ($E > 100$ keV) ions within the range $6\% < X[H_{\rm th}] < 20\%$.

Using the 3D ICRF wave propagation and absorption code LEMan [27], we have calculated the rf-power transferred to electrons and hydrogen as 11% and 89%, respectively, for the synergetic ICRF-NBI scenario. rf-wave fields are shown in Ref. [20]. Figure 3 compares the energetic distribution function across the ICRF heating schemes presented in previous work [6]. The comparison includes minority species ^{4}He(H) with ($X[H] = 2\%$), three-ion species H-(^{3}He)-^{4}He (with concentrations of 68%, 0.2%, and 15.9%, respectively), NBI only and the synergetic ICRF-NBI heating scenarios. All ICRF scenarios apply a dipole $(0,\pi)$ phasing at 1.5 MW with a dominant $k_{\|} = \pm 10$.

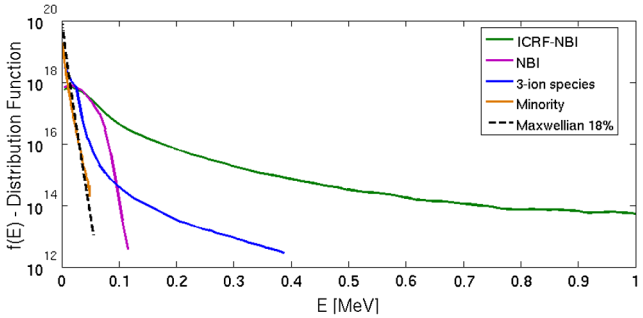

FIG. 3. Distribution function against energy for the W7-X high mirror equilibrium, comparing the ICRF-NBI synergetic heating with the standard NBI only and the minority and three-ion species ICRF-heating scenarios. The dotted line illustrates the number of particles present from a Maxwellian distribution of 18% concentration.

The number of particles around $E = 100$ keV is 2 orders of magnitude larger for the synergetic ICRF-NBI scheme than for the three-ion species ICRF-scheme. This clearly demonstrates the benefit of applying the synergetic ICRF-NBI method to investigate energetic ion physics in the high mirror W7-X equilibrium. The efficiency of the synergetic ICRF-NBI scheme as a heating method is measured by the power transferred to the background plasma. Figure 4 indicates significant improvement in the heating provided to the background plasma as compared with NBI only. The radial heating profile for the ICRF-NBI method indicates core-localized heating power where particle confinement is optimal. This is a significant improvement over ICRF-only schemes which typically have large edge power deposition, caused by two quasiomnigeneous stellarator specific factors: the toroidal magnetic mirror effect and the increased radial excursion of energetic deeply trapped ions, described in detail in Refs. [5,6]. As shown in Fig. 5(a), the energetic particle distribution of the three-ion species corresponds to trapped and deeply trapped particles ($\lambda = v_{\|}/v \to 0$) which result in larger radial diffusion and increased fast ion losses.

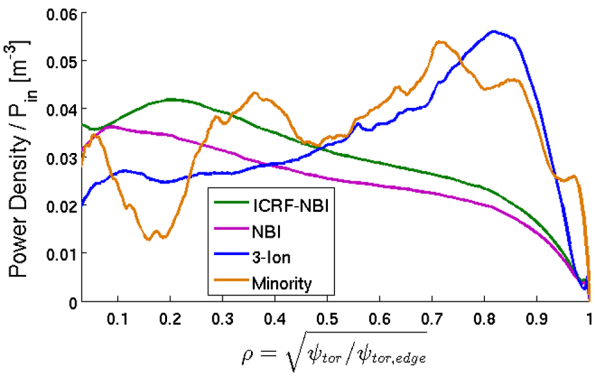

FIG. 4. Collisional power density transferred to the background plasma, normalized by the input powers: 1.5, 6.84, and 8.34 MW for ICRF only, NBI only, and ICRF-NBI heating, respectively.

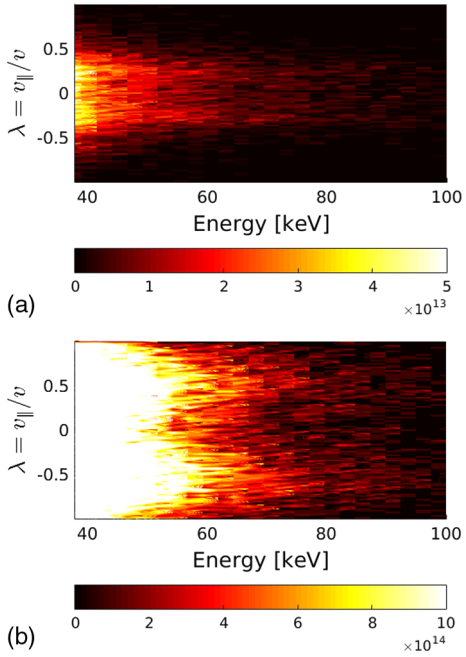

FIG. 5. Contour plot of the population of resonant ions against energy and pitch angle for (a) three-ion species and (b) Doppler-shifted resonance minority species synergetic ICRF-NBI heating schemes.

In contrast, the Doppler shifted synergetic minority species ICRF-NBI scheme in Fig. 5(b) illustrates a more isotropic, alphalike velocity distribution. It is found that 61% and 74% of energetic ($E > 70$ keV) ion losses had $|\lambda| < 0.2$ for the synergetic ICRF-NBI and three-ion species scheme, respectively. An improvement in energetic ($E > 15$ keV) NBI ion confinement occurs for the synergetic ICRF-NBI scheme over pure NBI of between 8%–29%, depending on the thermal NBI concentration $6\% < X[H_{\text{th}}] < 20\%$. However, Eq. (3) does not necessarily exhibit enhanced parallel velocity diffusion in the edge region, which results in larger NBI ion losses, though only for ion energies close to thermal values (between 4–15 keV). Improved plasma heating is therefore observed, as particles transfer more of their energy to the background plasma before being lost from the plasma.

To summarize, via fundamental analysis of the ICRF induced quasilinear velocity space diffusion, including code validation against neutron measurements from JET tokamak experiments, this Letter presents the application of the Doppler-shifted resonance minority species synergetic ICRF-NBI heating scheme to W7-X. For this specific synergetic ICRF-NBI scheme, the total NBI ion concentration is required to remain a minority and the background majority is of a different charge-to-mass ratio. The scheme applies an off-axis antenna frequency that compensates for the beam Doppler shift in order for ionized NBI ions to resonate on-axis. This modifies the diffusion of particles in velocity space through the quasilinear operator, increasing the particle velocity diffusion in the direction parallel to the magnetic field, reducing the fraction of deeply trapped resonant ions as compared to pure ICRF schemes. This subsequently leads to energetic particle generation up to the MeV range at concentrations orders of magnitude higher than the three-ion and minority species ICRF schemes also investigated here. Because of the less anisotropic velocity distribution as compared to pure NBI or pure ICRF heating, the synergetic ICRF-NBI scenario could be used for Alfvén eigenmode studies [28], fast ion loss studies due to low frequency MHD instabilities in the intrinsically strong 3D magnetic equilibrium, and crucially to mimic alpha particle confinement studies. This synergetic ICRF-NBI scheme also provides improved normalized core-localized heating over pure NBI, and thus could be used for high-performance plasma scenarios. The improved performance of the scheme over pure NBI and ICRF schemes is attributed to the low collisionality of the injected NBI ions, enhanced wave polarization over standard minority species schemes, and to the improved fast ion confinement through enhanced parallel velocity space diffusion. In the future, W7-X experimental diagnostics such as the neutron detector [29] and the fast ion loss detector [30] could be used to compare with these results.

The authors are grateful to D. Van Eester and E. Lerche for their helpful discussions on this work. This work has been carried out within the framework of the EUROfusion Consortium and has received funding from the Euratom research and training programme 2014–2018 and 2019–2020 under Grant Agreement No. 633053. The views and opinions expressed herein do not necessarily reflect those of the European Commission. The project was also supported in part by the Swiss National Science Foundation. The Piz Daint (CSCS, Switzerland) and the MARCONI-Fusion (CINECA/ENEA, Italy) supercomputer facilities were used for the simulations presented in this research. Numerical calculations using Piz Daint were supported by a grant from CSCS under project ID's s914 and s821.

[*] See the author list of the overview of the JET preparation for the deuterium-tritium operation by E. Joffrin *et al.*, Nucl. Fus., Special issue: Overview and summary reports from the 27th Fusion Energy Conference (Ahmedabad, India, 22–27 October 2018) (to be published).

[†] Present address: Department of Statistics, University of Oxford, OX1 3LB Oxford, United Kingdom.
hamish.patten@stats.ox.ac.uk

[1] T. Klinger *et al.*, Nucl. Fusion **59**, 112004 (2019).
[2] A. Dinklage *et al.*, Nat. Phys. **14**, 855 (2018).
[3] Y. I. Kolesnichenko, A. Könies, V. V. Lutsenko, M. Drevlak, Y. Turkin, and P. Helander, Nucl. Fusion **56**, 066004 (2016).
[4] Y. O. Kazakov, D. Van Eester, R. Dumont, and J. Ongena, Nucl. Fusion **55**, 032001 (2015).
[5] J. M. Faustin, W. A. Cooper, J. P. Graves, D. Pfefferlé, and J. Geiger, Plasma Phys. Controlled Fusion **58**, 074004 (2016).

[6] H. Patten, J. P. Graves, J. Faustin, W. A. Cooper, J. Geiger, D. Pfefferlé, and Y. Turkin, Plasma Phys. Controlled Fusion **60**, 085009 (2018).
[7] P. Helander *et al.*, Plasma Phys. Controlled Fusion **54**, 124009 (2012).
[8] N. Rust, B. Heinemann, B. Mendelevitch, A. Peacock, and M. Smirnow, Fusion Eng. Des. **86**, 728 (2011).
[9] M. Drevlak, J. Geiger, P. Helander, and Y. Turkin, Nucl. Fusion **54**, 073002 (2014).
[10] J. M. Faustin, W.A. Cooper, J. P. Graves, D. Pfefferlé, and J. Geiger, Nucl. Fusion **56**, 092006 (2016).
[11] J. Ongena *et al.*, EPJ Web Conf. **157**, 02006 (2017).
[12] M. Jucker, J. P. Graves, W. A. Cooper, N. Mellet, T. Johnson, and S. Brunner, Comput. Phys. Commun. **182**, 912 (2011).
[13] E. A. Lerche, D. Van Eester, A. Krasilnikov, J. Ongena, and P. Lamalle, Plasma Phys. Controlled Fusion **51**, 044006 (2009).
[14] C. Hellesen, M. Mantsinen, S. Conroy, G. Ericsson, J. Eriksson, V. G. Kiptily, and F. Nabais, Nucl. Fusion **58**, 056021 (2018).
[15] D. Gallart *et al.*, Nucl. Fusion **58**, 106037 (2018).
[16] R. Bilato, M. Brambilla, O. Maj, L. D. Horton, C. F. Maggi, and J. Stober, Nucl. Fusion **51**, 103034 (2011).
[17] E. A. Lerche *et al.*, Nucl. Fusion **56**, 036022 (2016).
[18] M. L. Mayoral *et al.*, Nucl. Fusion **46**, S550 (2006).
[19] Y. I. Kolesnichenko, V. V. Lutsenko, T. S. Rudenko, and P. Helander, Nucl. Fusion **57**, 066004 (2017).
[20] H. Patten, Development and optimisation of advanced auxiliary ion heating schemes for 3D fusion plasma devices, Ph.D. thesis 9167, École Polytechnique Fédérale de Lausanne, 2019, https://dx.doi.org/10.5075/epfl-thesis-9167.
[21] C. F. Kennel and F. Engelmann, Phys. Fluids **9**, 12 (1966).
[22] T. H. Stix, in *Waves in Plasmas 1992 Editon* (Springer, New York, 1992), pp. 501–503.
[23] M. Gatu Johnson *et al.*, Nucl. Instrum. Methods Phys. Res., Sect. A **591**, 417 (2008).
[24] D. Pfefferlé, Energetic ion dynamics and confinement in 3D saturated MHD configurations, Ph.D. thesis, École Polytechnique Fédérale de Lausanne, 2015, https://dx.doi.org/10.5075/epfl-thesis-6561.
[25] H. S. Bosch and G. M. Hale, Nucl. Fusion **32**, 611 (1992).
[26] H. S. Bosch, A. Dinklage, T. Klinger, R. Wolf, and Wendelstein -X Team, Contrib. Plasma Phys. **50**, 687 (2010).
[27] N. Mellet, W. A. Cooper, P. Popovich, L. Villard, and S. Brunner, Comput. Phys. Commun. **182**, 570 (2011).
[28] R. Dumont *et al.*, Nucl. Fusion **58**, 082005 (2018).
[29] W. Schneider, B Wiegel, F. Grünauer, R. Burhenn, S. Koch, H. Schuhmacher, and A. Zimbal, J. Instrum. **7**, C03025 (2012).
[30] K. Ogawa *et al.*, J. Instrum. **14**, C09021 (2019).